Porous Boron Carbon Nitride Nanosheets as Efficient Metal-Free Catalysts for the Oxygen Reduction Reaction in Both Alkaline and Acidic Solutions

Jiemin Wang, Jian Hao, Dan Liu, Si Qin, David Portehault, Yinwei Li, Ying Chen, Weiwei Lei

Porous Boron Carbon Nitride Nanosheets as Efficient Metal-free Catalysts for the Oxygen Reduction Reaction in Both Alkaline and Acidic Solutions

Jiemin Wang, Jian Hao, Dan Liu, Si Qin, David Portehault, Yinwei Li, Ying Chen, and Weiwei Lei

Just Accepted

Porous Boron Carbon Nitride Nanosheets as Efficient Metal-free Catalysts for the Oxygen Reduction Reaction in Both Alkaline and Acidic Solutions

Jiemin Wang,[†] Jian Hao,[†,‡] Dan Liu,*[†] Si Qin,[†] David Portehault,[§] Yinwei Li,[‡] Ying Chen[†] and Weiwei Lei*[†]

[†]Institute for Frontier Materials, Deakin University, 75 Pigdons Road, Waurn Ponds, 3216,VIC, Australia

Emails: weiwei.lei@deakin.edu.au; dan.liu@deakin.edu.au

[‡]School of Physics and Electronic Engineering, Jiangsu Normal University, Xuzhou,Jiangsu, 221116, China

[§]Sorbonne Universités, UPMC Université Paris 06, CNRS, Collège de France, Laboratoire de Chimie de la Matière Condensée de Paris (LCMCP), 11 place Marcelin Berthelot, F-75005 Paris, France

ABSTRACT: The carbon materials have become a hot topic as potential substitution of Pt/C catalysts for oxygen reduction reaction (ORR). However, most of them only prove their catalytic activities in alkaline solutions, which severely limit the applications in polyelectrolyte membrane fuel cells (PEMFCs). To address this issue, here porous boron carbon nitride (BCN) nanosheets are fabricated by a facile and efficient polymer sol-gel method, which involves the annealing of polyvinylic akohol (PVA), boric acid, guanidine and poly (ethylene oxide-co- propylene oxide) (P123) gel mixtures. The as-prepared porous BCN nanosheets possess a high surface area of 817 m^2/g and display impressive ORR catalytic performance in both alkaline and acid media, rivalling that of commercial Pt/C and other latest reported carbon materials. Importantly, the resulting metal-free catalysts exhibit much greater durability and higher methanol tolerance in both alkaline and acid environment as well. This study provides a new sight for metal-free ORR catalysts which are practicable in industrial fuel cells.

TOC GRAPHICS
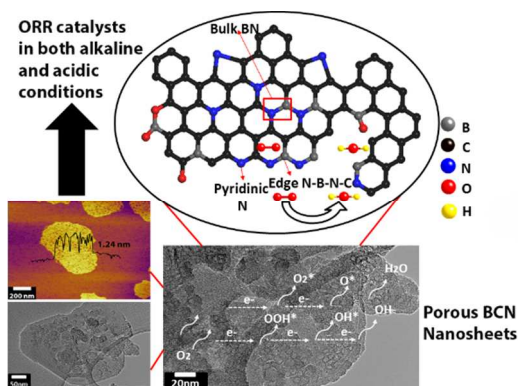
The ORR is pivotal in fuel cells and metal batteries.[1] In general, the noble metal Pt-based catalysts dominate in the ORR field owing to excellent electrocatalytic activity.[2] Nevertheless, the scarcity, easy deactivation by CO poisoning, fuel crossover effect, and low durability greatly impede the development of Pt based catalysts.[3-5] To address these issues, other materials such as transition-metal dichalcogenides[6] and carbon nanomaterials[7,8] are favoured as promising candidates. Among them, metal-free heteroatom-doped (such as B,N,S,P) carbon nanomaterials are predominate with superior ORR catalytic performance by providing not only large surface area but also more polarized active sites for oxygen adsorption or splitting.[9-11] However, most of them are mainly focused on behaviours in alkaline conditions. Only a few metal-free carbon nanomaterials catalysts can be affordable in the acidic media,[12-15] due to the poor durability and electroactivity deterioration. However, currently, most fuel cells are equipped with acid electrolyte.[4,12] Meanwhile, those carbon nanomaterials with benign behaviours in acid conditions are commonly functionalized with metal impurities or complexes,[16,17] which unavoidably increase the cost. Therefore, to cater for the current commercial market, the development of a practical metal-free heteroatom-doped carbon nanomaterial applicable in both alkaline and acid environments is a big challenge.

Previous research has witnessed the boost of graphene as prominent two-dimensional (2D) nanomaterial in the energy applications including energy storage and electrocatalysis,[5,18,19] related to its pronounced physiochemical and electronic properties with elegant planar geometry. Structurally analogous to graphene, 2D hexagonal boron nitride (h-BN) is of extensive interests as well. In spite of being a wide gap semiconductor, h-BN displays excellent thermal conductivity, chemical stability and mechanical properties in the applications of polymer composites,[20] hydrogen storage[21] and water cleaning.[22-25] Related to but different from either

graphene or h-BN, ternary boron carbon nitride (BCN) nanosheets are likely to possess striking performances by integrating the merits of both graphene and h-BN. Furthermore, it has been reported that the band gap (0-5.5eV) of BCN is tuneable via adjusting the content of each heteroelement.[26-28] In addition, heteropolar B, N bonding largely stimulates electroactivity, thus benefiting the versatility of BCN nanosheets in electro energy applications.[29-31] Up to now, BCN nanosheets have placed values on lithium-ion batteries,[32] oxygen reduction reaction (ORR),[33] hydrogen evolutions (HER)[34] and supercapacitors,[35] which rival those of other 2D nanomaterials. Although B, N doped CNTs,[36,37] graphene[38-40] or BCN nanostructures[41-45] have been reported as effective ORR catalysts in alkaline media, no research has proposed the ORR electrocatalysis by metal-free BCN in acid condition. Hence, it is a challenge to developing a BCN-based nanostructured electrocatalyst performing not only in alkaline, but also in acid environment.

Herein, we design a simple and efficient polymer sol-gel method to prepare porous BCN nanosheets. In contrast with other traditional methods such as chemical vapor deposition (CVD), and microwave plasma CVD,[46,47] this route is of large scale production, low cost, and does not require high energy, vacuum systems and catalysts. The as-obtained BCN nanosheets reveal a high surface area of 817 m^2/g with both meso and micro pores. Our BCN catalysts demonstrate impressive ORR catalytic performances in both alkaline and acid conditions, comparable to Pt/C and other carbon nanomaterials ever reported. In addition, the products also manifest great long-term stability and better tolerance to the methanol crossover effect in both alkaline and acid media than commercial Pt/C. Obviously, the BCN nanosheets with porous nanostructure pave a potential way for substitution of Pt/C as effective metal-free ORR catalysts in industrial fuel cells.
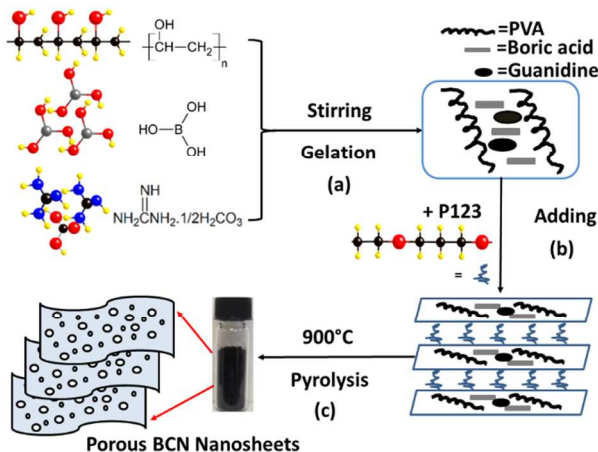
Scheme 1. Schematic synthesis process of porous BCN nanosheets including: (a) The gelation of polymer precursor. (b) The adding of P123 and (c) The pyrolysis at 900°C under N_2.

The synthetic strategy is schematically illustrated in Scheme 1. Firstly, the polymeric gel precursor is formed by hydroxyl and amino group crosslinking between polyvinylic akohol (PVA), boric acid and guanidine carbonate salt. Then the polymeric precursor is further cured by introduction of P123 for both porosity development[48,49] and nanosheets morphology control under the carbonation process.[50] After annealing at 900°C in N_2, the precursor gel architecture is gradually converted into a 2D porous layered structure and B, N, C atoms are mutually bonded upon carbonization. Finally the porous BCN nanosheets are generated in a mass scale.
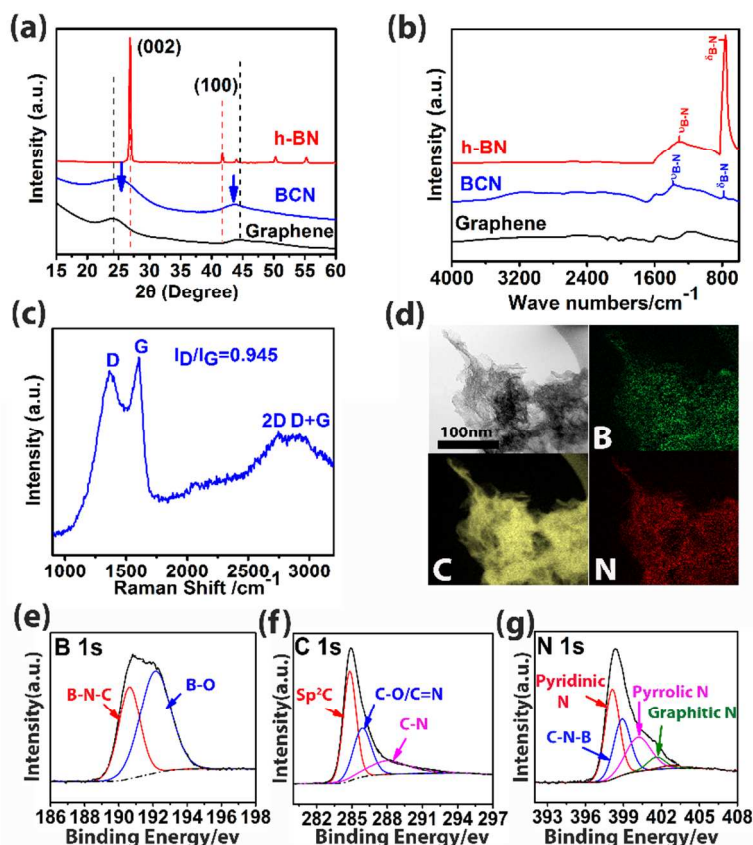
Figure 1. Characterization of the porous BCN nanosheets. a) XRD, b) FTIR and c) Raman of BCN nanosheets. d) TEM image of BCN nanosheets and corresponding EDS mapping of B,C,N elements, e) XPS B 1s spectrum, f) XPS C1s spectrum and g) XPS of N 1s spectrum of BCN nanosheets.

The X-Ray Diffraction (XRD) pattern (Figure 1a) suggests two characteristic peaks at around 26°and 43° respectively, typically representing (002) and (101) interlayers reflections of BCN.[26] Compared with reference h-BN and graphene, these intervenient shifting broad humps of (002) and (101) imply the presence of defects[28] and existence of sp^2-bonded conjugated graphitic carbons containing structural heteroatoms integrated within small stacks.[51] In the Fourier Transform Infrared (FTIR) spectrum (Figure 1b), two small bands at around 1380cm^{-1} and 900cm^{-1} could be attributed to B-N stretching bands (ν_{B-N}) and B-N bending bands (δ_{B-N}) respectively.

Evidently, these two bands show a little blue shift in contrast with that of h-BN, highlighting the conjugative effect of C-N-B in the ternary system.[38,39] The Raman spectrum (Figure 1c)

shows the characteristic signals of the D and G bands at around 1360 cm^{-1} and 1600cm^{-1} as well as two weak 2D and D+G bands at 2668 and 2900 cm^{-1}, consistent with previously reported BCN nanosheets.[47] A typical shift of the G band (1600cm^{-1}) in BCN is observed from pure graphene (1580cm^{-1}), attributing to the structural distortion of graphitic carbon with different bond lengths of N-B and C-N.[41] Besides, the appearance of relatively weak 2D band indicates the presence of a few layers in BCN nanosheets,[46] conforming to XRD analysis. Noticeably, the relative intensity of I_D/I_G, which represents the level of defects and heteroatom doping,[52] is 0.945 in this study, less than most of the B,N co-doped graphene (I_D/I_G >1)[38-45]. On one hand, it suggests that local structures of our BCN nanosheets evolve towards graphitization instead of highly defective and disordered heterojunctions.[45,51] On the other hand, the balance of electroactive defects and conductive ordered domains might be optimized in our sample, facilitating the electrochemical activities to the most extent.[4,49] Energy-dispersive spectroscopy (EDS) mapping (Figure 1d) and X-ray photoelectron spectroscopy (XPS) (Figure 1e-g and Figure S1) further demonstrate the existence of B, C and N elements in our sample. From EDS images, it is clear that all the elements (B,C and N) are distributed in the nanosheets evenly. The atomic concentration ratio of BCN is calculated to be $B_1C_{6.66}N_{1.09}$ (B: 11.48 at.%, C: 76.02 at.%, N: 12.50 at.%) from XPS results. The B1s spectra (Figure 1e) could be deconvoluted into two different signals at around 190.6eV and 192.1eV, indicating the coexistence of B-N-C and B-O bonds accordingly.[35,44,53,54] The C1s spectrum in Figure 1f highlights that sp^2 C=C bonding (at ~284.7eV) dominates in the whole BCN conjugated frame. Other two smaller C 1s peaks at about 286eV and 289eV are corresponding to C-O/C-N and C=N bonds respectively.[26,35,38] Moreover, the deconvolution of high-resolution N1s band describes four types of N species including pyridinic N (~398.2eV), pyrrolic N (~400.4eV), quaternary N (~401.4eV) and C-N-

B(~399eV) separately (Figure 1g).[35,55] Interestingly, pyridinic N accounts for the highest

percentage (38.64 at.%) in the N atomic concentration, followed by C-N-B bonding (27.6 at.%),

implying that a large number of ORR active sites exists in our BCN nanosheets.[43,56,57] In

agreement with XRD, Raman and FTIR, the XPS results demonstrate the successful synthesis of

BCN nanosheets. In addition, the potential complementary effects of B and N atoms as well as

adjustable electronic structure of carbon should greatly benefit the electrochemical activity as

ORR catalysts.[27]
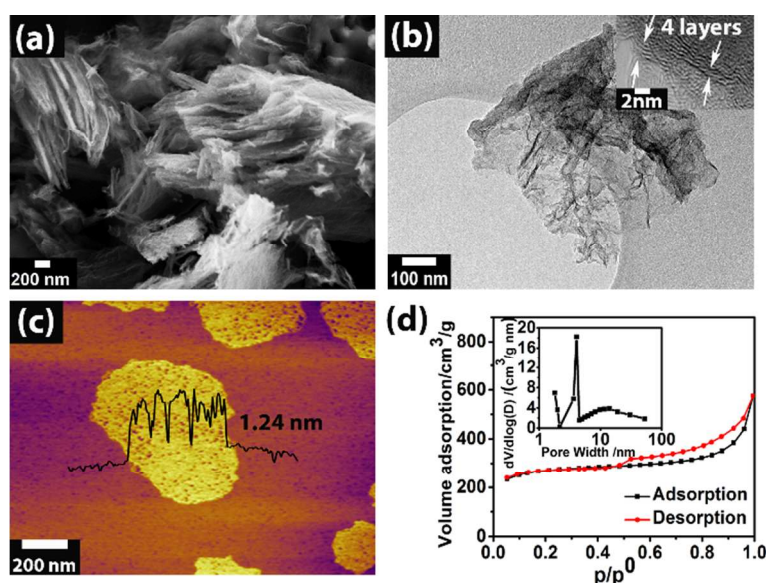
Figure 2. Morphologies of the porous BCN nanosheets. a) SEM, b) TEM and c) AFM pictures of BCN nanosheets. Inset of (b) shows the edge folding of the BCN sheet with 3-5 layers. d) Nitrogen adsorption/desorption isotherms of BCN nanosheets, the inset shows the corresponding pore size distributions.

Scanning electron microscope (SEM) displays the fluffy, thin and stacked lamellar

architectures of BCN nanosheets as shown in Figure 2a. This is also confirmed in Transmission

Electron Microscopy (TEM) images (Figure 2b), in which a crumpled lamellar structure could be

seen clearly. High-resolution TEM (HRTEM) (Inset of Figure 2b) discloses 3-5 parallel fringes

on the folded edge of the nanosheets, suggesting 3-5 layers contained in the nanosheets. In

addition, some wrinkled fringes on the nanosheets reveal a little disorder of the crystallization,

corresponding to the XRD results. The interlayer distance is about 0.35nm, well in accordance with the interplane (002) spacing of BCN.[33] The Atomic Force Microscope (AFM) results (Figure 2c) further confirm the layered structure of BCN with a uniform thickness of 1.24nm, conforming to 3-4 stacked layers. Besides, a holey structure of BCN nanosheets could be well discerned in the AFM image (Figure S4), which could also be observed in the TEM image (Figure S2). The surface area and porosity of the materials are studied by Brunauer-Emmett-Teller (BET) test. In Figure 2d, the nitrogen adsorption–desorption isotherms suggest a type IV curve with a visible H3 type hysteresis loop, demonstrating the presence of a size distribution of mesopores in the range of relative pressure 0.5-1.0.[22] The BET surface area and the total pore volume are calculated to be $817m^2/g$ and $0.624cm^3/g$ respectively, larger than previously reported gelatin derived BCN nanosheets ($416m^2/g$).[35] It is worth noting that soft templates P123 would lead to hydrogen bonding bridge in the polymer gel precursors, giving rise to more gaseous oxygen containing groups among chains in contrast with no P123 cured precursor (FigureS5). In the synthesis, some gases such as CO, CO_2 and NH_3 are released through the spaces between layers during decomposition. Thus a larger number of pores are finally achieved.[48,49] The results implicate that such a porous structure of nanosheets with relative high BET surface could promote the ORR catalytic activities to a large extent.

Figure 3. ORR catalytic performance of the porous few-layered BCN in 0.1M KOH. a) LSV curves of BCN catalysts and Pt/C at a rotation rate of 1600 rpm and a scan rate of 5mV/s. The inset shows the higher magnification of LSV curves between 0.9-1.0V *vs*. RHE. b) LSV curves of BCN catalysts with various rotation rates from 400 rpm-2500 rpm at a scan rate of 5 mV/s. The inset shows the corresponding Koutecky–Levich plot. c) RRDE voltammograms and d) H_2O_2 yield corresponding to the total oxygen reduction products and the calculated electron transfer number of few-layered BCN. e) Chronoamperometric measurement for few-layered BCN and Pt/C in an O_2-saturated 0.1 M KOH solution and when 3.0 M methanol is added at around 300 s at an electrode rotation rate of 1600 rpm. f) Current–time chronoamperometric

response of few-layered BCN and Pt/C in an O_2-saturated 0.1 M KOH solution at a rotation rate of 1600 rpm.

The ORR activity of the as-synthesized BCN nanosheets is investigated under alkaline condition (0.1M KOH) firstly. A Cyclic voltammetry (CV) (Figure S7a) reveals a well-defined and strong cathodic ORR peak at around 0.8V vs. RHE, indicating the high catalytic activity of BCN nanosheets in alkaline environment. In addition, as shown in Figure3a, the onset potential (E_{onset}) of the porous BCN nanosheets is 0.940V *vs*. RHE, only 13mV less than 20% Pt/C (0.953V *vs*. RHE). And the half-wave potential ($E_{1/2}$) is 0.82V *vs*. RHE, which is dramatically close to that of Pt/C (0.84V *vs*. RHE) as well.[12] Notably, the ORR activity of our sample is better than several other reported B,N dual doped graphene or BCN nanomaterials with either E_{onset}, $E_{1/2}$ or both potential being more positive (Table S1).[36-45] The number (n) of electrons transferred per O_2 molecule is estimated to be 3.91 at 0.364 V *vs*. RHE according to the Koutecky–Levich (K-L) plot built from the linear sweep voltammetry (LSV) curves under different electrode rotating speeds (Figure 3b),[51,52] thus indicating a 4e⁻ pathway for ORR. To further study the ORR performance in 0.1M KOH, the rotating ring-disk electrode (RRDE) measurement is conducted. Figure 3c displays both disk and ring currents for BCN nanosheets. The average electron number is measured to be 3.93 (Figure 3d), verifying the 4e⁻ oxygen reduction selectivity again, well conforming to the results obtained from K-L plot. Furthermore, the calculated H_2O_2 yield is below 6%, suggesting an efficient 4e⁻ pathway ORR catalytic behavior. Moreover, the porous BCN nanosheets exhibit an outstanding tolerance for methanol cross-over effect (Figure 3f) and impressive long term durability (Figure 3d), which are both superior to commercial 20% Pt/C.
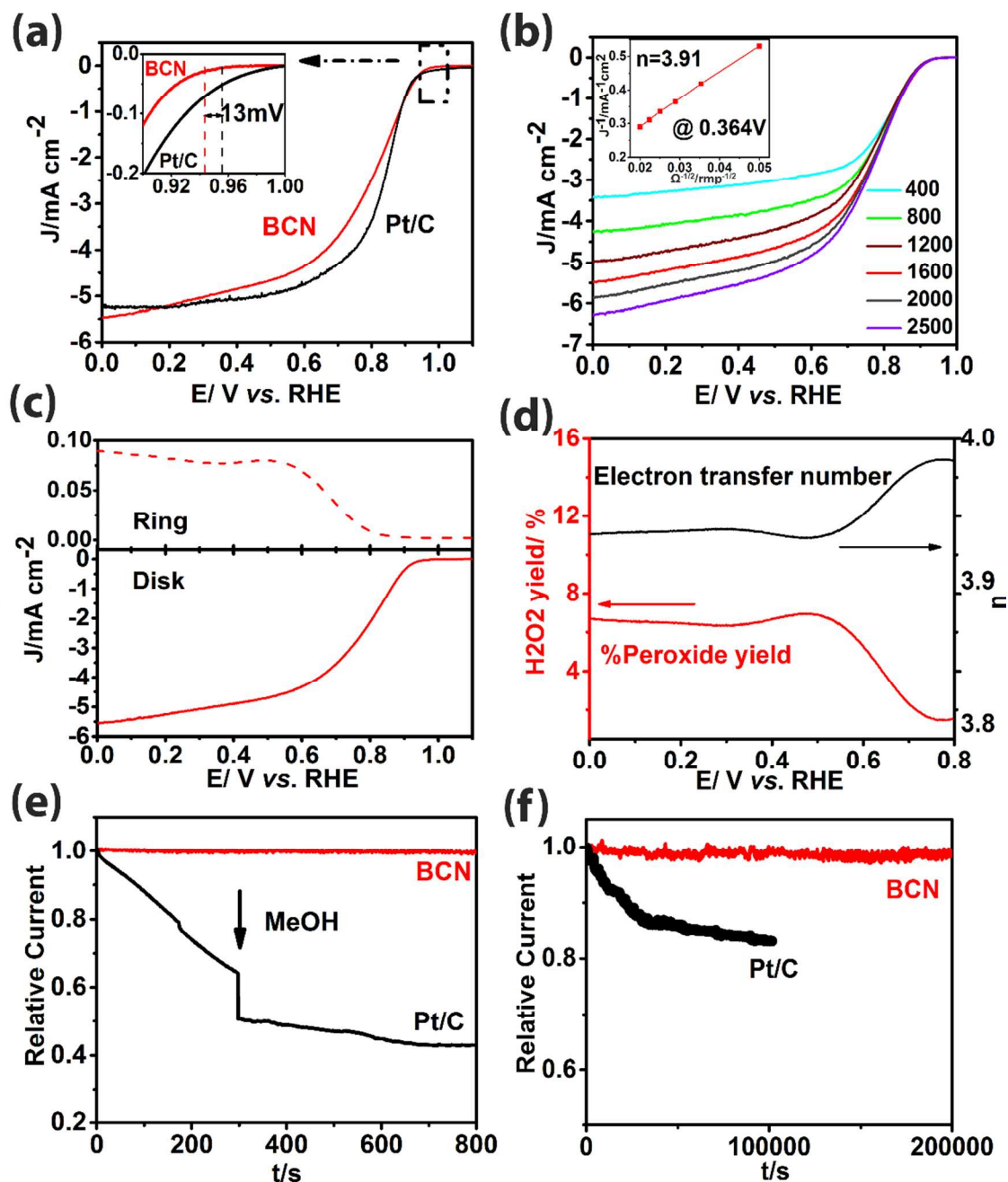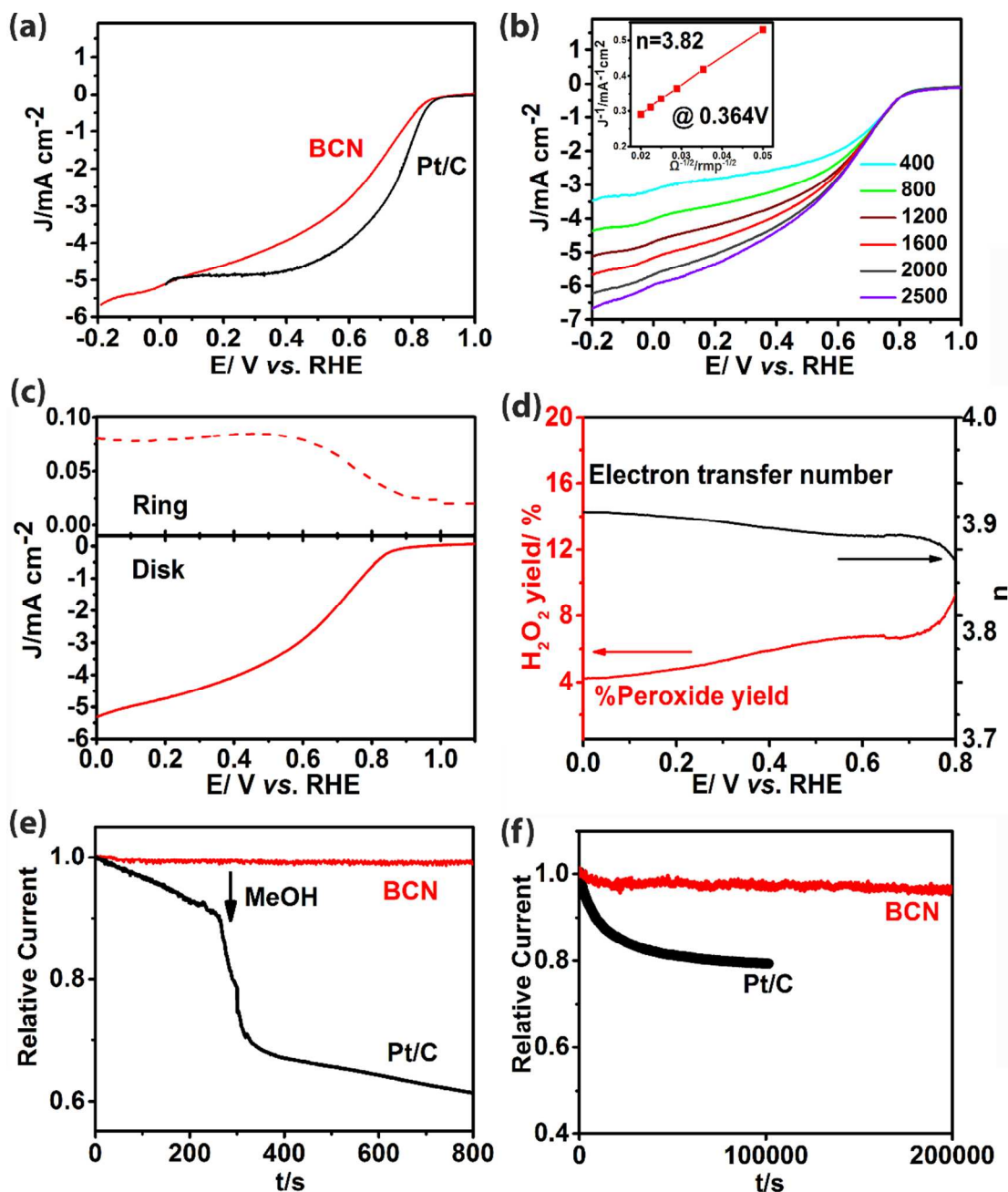
Figure 4. ORR catalytic performance of the porous few-layered BCN in 0.1M HClO$_4$. a) LSV curves of BCN catalysts and Pt/C at a rotation rate of 1600 rpm and a scan rate of 5mV/s. b) LSV curves of BCN catalysts with various rotation rates from 400 rpm-2500 rpm at a scan rate of 5 mV/s. The inset shows the corresponding Koutecky–Levich plot. c) RRDE voltammograms and d) H$_2$O$_2$ yield corresponding to the total oxygen reduction products and the calculated electron transfer number of few-layered BCN. e) Chronoamperometric measurement for few-layered BCN and Pt/C in an O$_2$-saturated 0.1 M HClO$_4$ solution and when 3.0 M methanol is added at around 300 s at an electrode rotation rate of 1600 rpm. f) Current–time chronoamperometric response of few-layered BCN and Pt/C in an O$_2$-saturated 0.1 M HClO$_4$ solution at a rotation rate of 1600 rpm.

It is of great importance that the as-obtained BCN catalysts also exhibit excellent ORR activity and stability in acidic 0.1M $HClO_4$. A distinct cathodic peak could be clearly observed in Figure S7b. Although the onset potential (E_{onset}) of our BCN catalyst (0.84V *vs.* RHE) is slightly less than Pt/C (0.93V *vs.* RHE) in Figure 4a, it is fully comparable and even better than the most recently reported state-of-the-art carbon materials including heteroatoms doped CNT/graphene or Fe/N doped CNTs in acid environment (See Table S2).[12-17] Besides, the K-L plot in Figure 4b inset (n=3.82 at 0.364V *vs.* RHE) and RRDE measurement results in Figure 4c and d (average n=3.88) both confirm a 4e⁻ transfer route for BCN nanosheets in 0.1M $HClO_4$. Furthermore, the peroxide yield is lower than 8% at all potentials, disclosing the high O_2 reduction selectivity even in acid condition. More significantly, the nearly unchanged durability and tolerance for MeOH cross-over effect (Figure 4e and 4f) demonstrate the feasibility of the porous BCN nanosheets as potential candidates in PEM fuel cells again.

In respect to the chemical compositional, structural and morphological characterizations of the porous BCN nanosheets, the superior ORR catalytic activity and stability could be ascribed to several aspects. Firstly, high concentration of pyridinic N (38.64%) doped into the nanosheets could accelerate O_2 adsorption by reducing the local work function and providing more Lewis base sites next to carbon, which are energetically favoured as adsorption sites by oxygen molecules.[50,56] Therefore, the number of the activated carbon atoms are boomed with the nitrogen doping.[57,58] Secondly, recent studies reveal that B-N-C edge groups play a crucial role to enhance the ORR performance.[27,40] Notably, although isolated BN domains are inactive as the ORR catalysts,[37,39] the edge B-N-C groups may boost the ORR catalytic activity. In our sample, it is likely that abundant B-N-C (27.6 at.%) bonding is easily accessible to OH adsorption and O protonation in the graphitic carbon edge area.[53,55] As a consequence, the ORR activity is further

presumably improved at B-N-C edge. Thirdly, heteropolar B-N bonding as well as ionized B-O bonds provides an extra dipole, thereby likely enhancing the relative wettability (hydrophilicity) between electrolyte and electrode materials and develops a faster O_2 transfer kinetic mechanism.[29-31] Furthermore, the large surface area facilitates more active sites. The micropores and mesopores in our sample are able to support a shorter ion-transport pathway, preferably realizing the exchange of molecules and ions in the electrolytes.[30] In addition, although the ORR catalytic performance in acid environment is inferior to that of alkaline, the difference is relatively minor in contrast with some of other carbon materials.[12-16] For single nitrogen-doped carbon materials in low pH solutions, the increased proton concentration degrades the ORR reaction kinetics with the protonation of negatively charged N atoms.[59] However, for BCN nanosheets, the positively charged B atoms might alleviate the effect of protonation process, thereby narrowing the gap of ORR catalytic activity between alkaline and acid environment. Briefly, the stimulative B, N dual-doping effects discussed above and the 2D nanostructure with hierarchical porosity make our BCN nanosheets a remarkable low-cost and highly efficient ORR metal-free catalysts in both alkaline and acid media.

In summary, we have designed a novel, simple, and scalable polymer sol-gel approach to directly synthesize porous and few-layered BCN nanosheets. The B, N co-doping, 2D-nanostructure and high surface area with rational porosity enable the BCN nanosheets to be efficient as ORR catalysts. In the alkaline medium, the sample displays comparable activity, greater methanol durability and better stability than 20% Pt/C. More importantly, the as-obtained catalysts also demonstrate considerable ORR performance in strong acid environment, superior to some other carbon materials. Therefore, this study provides an effective method to construct

new BCN nanomaterials as high-efficiency metal-free ORR electrocatalysts in both alkaline and acid conditions, which could satisfy the greater desire of commercial PEMFCs.

ASSOCIATED CONTENT

Supporting Information.

Experimental details, Figures of XPS Survey Spectra of the porous BCN nanosheets, TEM, SEM and AFM images of the porous BCN nanosheets, Nitrogen adsorption/desorption isotherms and TEM images of BCN nanosheets synthesized without adding P123, CV curves of BCN nanosheets for ORR in N_2 and O_2 saturated solution in 0.1M KOH solution and 0.1M $HClO_4$ solution. RDE linear sweep voltammograms (LSV) curves of graphite+BN (mole ratios=6.7:1), pure graphite and BCN at a rotation rate of 1600 rpm and a scan rate of 5mV/s in 0.1M KOH solution. Table of comparison of several reported B,N-doped graphene and borocarbonitride nanosheets as ORR catalysts in alkaline conditions, Table of comparison of latest reported carbon materials (metal free and Fe containing) with high ORR performances in acid solutions.

AUTHOR INFORMATION

Email: weiwei.lei@deakin.edu.au

REFERENCES

(1) Xia,W.; Liang, Z.; Zou, R.; Guo, S. Earth−abundant nanomaterials for oxygen reduction. *Angew. Chem., Int. Ed.* **2015***, 54,* 2–29.

(2) Wang, D.; Xin, H. L.; Hovden, R.; Wang, H.; Yu, Y.; Muller, D. A.; DiSalvo, F. J.; Abruna, H. D. Structurally ordered intermetallic platinum-cobalt core-shell nanoparticles with enhanced activity and stability as oxygen reduction electrocatalysts. *Nature mater.* **2013,** *12*, 81-87.

(3) Nie, Y.; Li, L.; Wei, Z. Recent advancements in Pt and Pt-free catalysts for oxygen reduction reaction. *Chem. Soc. Rev.* **2015,** *44*, 2168-2201.

(4) Zhou, M.; Wang, H. L.; Guo, S. Towards high-efficiency nanoelectrocatalysts for oxygen reduction through engineering advanced carbon nanomaterials. *Chem. Soc. Rev.* **2016,** *45*, 1273-1307.

(5) Geng, D.; Ding, N.; Andy Hor, T. S.; Liu, Z.; Sun, X.; Zong, Y. Potential of metal-free "graphene alloy" as electrocatalysts for oxygen reduction reaction. *J. Mater. Chem. A* **2015,** *3*, 1795-1810.

(6) Chia, X.; Eng, A. Y. S.; Ambrosi, A.; Tan, S. M.; Pumera, M. Electrochemistry of nanostructured layered transition-metal dichalcogenides. *Chem. Rev.* **2015,** *115*, 11941-11966.

(7) Sa, Y. J.; Park, C.; Jeong, H. Y.; Park, S. H.; Lee, Z.; Kim, K. T.; Park, G. G.; Joo, S. H. Carbon nanotubes/heteroatom-doped carbon core-sheath nanostructures as highly active, metal-free oxygen reduction electrocatalysts for alkaline fuel cells. *Angew. Chem., Int. Ed.* **2014,** *53*, 4102-4106.

(8) Ye, T.; Lv, L.; Li, X.; Xu, M.; Chen, J. Strongly veined carbon nanoleaves as a highly efficient metal-free electrocatalyst. *Angew. Chem., Int. Ed.* **2014,** *53*, 6905-6909.

(9) Zhao, Z.; Li, M.; Zhang, L.; Dai, L.; Xia, Z. Design principles for heteroatom-doped carbon nanomaterials as highly efficient catalysts for fuel cells and metal-air batteries. *Adv. mater.* **2015,** *27*, 6834-6840.

(10) Wang, X.; Sun, G.; Routh, P.; Kim, D. H.; Huang, W.; Chen, P. Heteroatom-doped graphene materials: syntheses, properties and applications. *Chem. Soc. Rev.* **2014,** *43*, 7067-7098.

(11) Jiao, Y.; Zheng, Y.; Jaroniec, M.; Qiao, S. Z. Origin of the electrocatalytic oxygen reduction activity of graphene-based catalysts: a roadmap to achieve the best performance. *J. Am. Chem. Soc.* **2014,** *136*, 4394-4403.

(12) Shui,J. M. W., Du, F.; Dai, L. N-doped carbon nanomaterials are durable catalysts for oxygen reduction reaction in acidic fuel cells. *Sci. Adv.* **2015,** *10*, 444-448.

(13) Zhang, J.; Zhao, Z.; Xia, Z.; Dai, L. A metal-free bifunctional electrocatalyst for oxygen reduction and oxygen evolution reactions. *Nature Nanotech.* **2015,** *10*, 444-452.

(14) Yang, J.; Sun, H.; Liang, H.; Ji, H.; Song, L.; Gao, C.; Xu, H. A highly efficient metal-free oxygen reduction electrocatalyst assembled from carbon nanotubes and graphene. *Adv. mater.* **2016,** *28*, 4606-4613.

(15) Wei, W.; Liang, H.; Parvez, K.; Zhuang, X.; Feng, X.; Mullen, K. Nitrogen-doped carbon nanosheets with size-defined mesopores as highly efficient metal-free catalyst for the oxygen reduction reaction. *Angew. Chem., Int. Ed.* **2014,** *53*, 1596-1600.

(16) Li, Y.; Zhou, W.; Wang, H.; Xie, L.; Liang, Y.; Wei, F.; Idrobo, J. C.; Pennycook, S. J.; Dai, H. An oxygen reduction electrocatalyst based on carbon nanotube-graphene complexes. *Nature Nanotech.* **2012,** *7*, 394-400.

(17) Lv, H.; Li, D.; Strmcnik, D.; Paulikas, A. P.; Markovic, N. M.; Stamenkovic, V. R. Recent advances in the design of tailored nanomaterials for efficient oxygen reduction reaction. *Nano Energy* **2016**, DOI:10.1016/j.nanoen.2016.04.008.

(18) Chabot, V.; Higgins, D.; Yu, A.; Xiao, X.; Chen, Z.; Zhang, J. A review of graphene and graphene oxide sponge: material synthesis and applications to energy and the environment. *Energy Environ. Sci.* **2014,** *7*, 1564-1596.

(19) Zhou, X.; Qiao, J.; Yang, L.; Zhang, J. A review of graphene-based nanostructural materials for both catalyst supports and metal-free catalysts in PEM fuel cell oxygen reduction reactions. *Adv. Energy Mater.* **2014,** *4*, 1301523, DOI: 10.1002/aenm.201301523.

(20) Liu, D.; He, L.; Lei, W.; Klika, K. D.; Kong, L.; Chen, Y. Multifunctional polymer/porous boron nitride nanosheet membranes for superior trapping emulsified oils and organic molecules. *Adv. Mater. Interfaces* **2015,** *2*, 1500228.

(21) Lei, W.; Zhang, H.; Wu, Y.; Zhang, B.; Liu, D.; Qin, S.; Liu, Z.; Liu, L.; Ma, Y.; Chen, Y. Oxygen-doped boron nitride nanosheets with excellent performance in hydrogen storage. *Nano Energy* **2014,** *6*, 219-224.

(22) Lei, W.; Portehault, D.; Liu, D.; Qin, S.; Chen, Y. Porous boron nitride nanosheets for effective water cleaning. *Nat. Commun.* **2013,** *4*, 1777-1784.

(23) Liu, D.; Lei, W.; Qin, S.; Klika, K. D.; Chen, Y. Superior adsorption of pharmaceutical molecules by highly porous BN nanosheets. *Phys. Chem. Chem. Phys.* **2016,** *18*, 84-88.

(24) Lei, W.; Liu, D.; Chen, Y. Highly crumpled boron nitride nanosheets as adsorbents: scalable solvent-less production. *Adv. Mater. Interfaces* **2015,** *2*, 1400529.

(25) Liu, D.; Lei, W.; Qin, S.; Chen, Y. Template-free synthesis of functional 3D BN architecture for removal of dyes from water. *Sci. rep.* **2014,** *4*, 4453.

(26) Lei,W.; Portehault, D.; Dimova, R.; Antonietti, M. Boron carbon nitride nanostructures from salt melts: tunable water-soluble phosphors. *J. Am. Chem. Soc.* **2011,** *133*, 7121-7127.

(27) Wu, J.; Rodrigues, M. F.; Vajtai, R.; Ajayan, P. M. Tuning the electrochemical reactivity of boron- and nitrogen-substituted graphene. *Adv. mater.* **2016**, *28*, 6239–6246.

(28) Kumar, N.; Moses, K.; Pramoda, K.; Shirodkar, S. N.; Mishra, A. K.; Waghmare, U. V.; Sundaresan, A.; Rao, C. N. Borocarbonitrides, BxCyNz. *J. Mater. Chem. A* **2013,** *1*, 5806-5813.

(29) Wu, Z.; Ren, W.; Xu, L.; Li, F.; Cheng, H. Doped graphene sheets as anode materials with super high rate and large capacity for lithium ion batteries. *ACS Nano* **2011,** *5*, 5463-5471.

(30) Guo, H.; Gao, Q. Boron and nitrogen co-doped porous carbon and its enhanced properties as supercapacitor. *J. Power Sources* **2009,** *186*, 551-556.

(31) Konno, H.; Ito, T.; Ushiro, M.; Fushimi, K.; Azumi, K. High capacitance B/C/N composites for capacitor electrodes synthesized by a simple method. *J. Power Sources* **2010,** *195*, 1739-1746.

(32) Lei, W.; Qin, S.; Liu, D.; Portehault, D.; Liu, Z.; Chen, Y. Large scale boron carbon nitride nanosheets with enhanced lithium storage capabilities. *Chem. commun.* **2013,** *49*, 352-354.

(33) Moses, K.; Kiran, V.; Sampath, S.; Rao, C. N. Few-layer borocarbonitride nanosheets: platinum-free catalyst for the oxygen reduction reaction. *Chem. Asian J.* **2014,** *9*, 838-843.

(34) Chhetri, M.; Maitra, S.; Chakraborty, H.; Waghmare, U. V.; Rao, C. N. Superior performance of borocarbonitrides, BxCyNz, as stable, low-cost metal-free electrocatalysts for the hydrogen evolution reaction. *Energy Environ. Sci.* **2016,** *9*, 95-101.

(35) Ling, Z.; Wang, Z.; Zhang, M.; Yu, C.; Wang, G.; Dong, Y.; Liu, S.; Wang, Y.; Qiu, J. Sustainable synthesis and assembly of biomass-derived B/N co-doped carbon nanosheets with ultrahigh aspect ratio for high-performance supercapacitors. *Adv. Funct. Mater.* **2016,** *26*, 111-119.

(36) Wang, S.; Iyyamperumal, E.; Roy, A.; Xue, Y.; Yu, D.; Dai, L. Vertically aligned BCN nanotubes as efficient metal-free electrocatalysts for the oxygen reduction reaction: a synergetic effect by co-doping with boron and nitrogen. *Angew. Chem., Int. Ed.* **2011,** *50*, 11756-11760.

(37) Zhao, Y.; Yang, L.; Chen, S.; Wang, X.; Ma, Y.; Wu, Q.; Jiang, Y.; Qian, W.; Hu, Z. Can boron and nitrogen co-doping improve oxygen reduction reaction activity of carbon nanotubes? *J. Am. Chem. Soc.* **2013,** *135*, 1201-1204.

(38) Wang, S.; Zhang, L.; Xia, Z.; Roy, A.; Chang, D. W.; Baek, J. B.; Dai, L. BCN graphene as efficient metal-free electrocatalyst for the oxygen reduction reaction. *Angew. Chem., Int. Ed.* **2012,** *51*, 4209-4212.

(39) Zheng, Y.; Jiao, Y.; Ge, L.; Jaroniec, M.; Qiao, S. Z. Two-step boron and nitrogen doping in graphene for enhanced synergistic catalysis. *Angew. Chem., Int. Ed.* **2013,** *52*, 3110-3116.

(40) Gong, Y.; Fei, H.; Zou, X.; Zhou, W.; Yang, S.; Ye, G.; Liu, Z.; Peng, Z.; Lou, J.; Vajtai, R. *et al.* Boron- and nitrogen-substituted graphene nanoribbons as efficient catalysts for oxygen reduction reaction. *Chem. Mater.* **2015,** *27*, 1181-1186.

(41) Xue, Y.; Yu, D.; Dai, L.; Wang, R.; Li, D.; Roy, A.; Lu, F.; Chen, H.; Liu, Y.; Qu, J. Three-dimensional B,N-doped graphene foam as a metal-free catalyst for oxygen reduction reaction. *Phys. Chem. Chem. Phys.* **2013,** *15*, 12220-12226.

(42) Wang, Z.; Cao, X.; Ping, J.; Wang, Y.; Lin, T.; Huang, X.; Ma, Q.; Wang, F.; He, C.; Zhang, H. Electrochemical doping of three-dimensional graphene networks used as efficient electrocatalysts for oxygen reduction reaction. *Nanoscale* **2015,** *7*, 9394-9398.

(43) Shi, Q.; Lei, Y.; Wang, Y.; Wang, H.; Jiang, L.; Yuan, H.; Fang, D.; Wang, B.; Wu, N.; Gou, Y. B, N-codoped 3D micro-/mesoporous carbon nanofibers web as efficient metal-free catalysts for oxygen reduction. *Curr. Appl. Phys.* **2015,** *15*, 1606-1614.

(44) Jiang, Z.; Zhao, X.; Tian, X.; Luo, L.; Fang, J.; Gao, H.; Jiang, Z. J. Hydrothermal synthesis of boron and nitrogen codoped hollow graphene microspheres with enhanced electrocatalytic activity for oxygen reduction reaction. *ACS Appl. Mater. Interfaces* **2015,** *7*, 19398-19407.

(45) Wang, L.; Yu, P.; Zhao, L.; Tian, C.; Zhao, D.; Zhou, W.; Yin, J.; Wang, R.; Fu, H. B and N isolate-doped graphitic carbon nanosheets from nitrogen-containing ion-exchanged resins for enhanced oxygen reduction. *Sci. Rep.* **2014,** *4*, 5184.

(46) Ci, L.; Song, L.; Jin, C.; Jariwala, D.; Wu, D.; Li, Y.; Srivastava, A.; Wang, Z. F.; Storr, K.; Balicas, L.; Liu *et al.* Atomic layers of hybridized boron nitride and graphene domains. *Nature Mater.* **2010,** *9*, 430-435.

(47) Qin, L.; Yu, J.; Kuang, S.; Xiao, C.; Bai, X. Few-atomic-layered boron carbonitride nanosheets prepared by chemical vapor deposition. *Nanoscale* **2012,** *4*, 120-123.

(48) Li, J.; Xiao, X.; Xu, X.; Lin, J.; Huang, Y.; Xue, Y.; Jin, P.; Zou, J.; Tang, C. Activated boron nitride as an effective adsorbent for metal ions and organic pollutants. *Sci. Rep.* **2013,** *3*, 3208.

(49) Bayatsarmadi, B.; Zheng, Y.; Jaroniec, M.; Qiao, S. Z. Soft-templating synthesis of N-doped mesoporous carbon nanospheres for enhanced oxygen reduction reaction. *Chem. Asian J.* **2015,** *10*, 1546-1553.

(50) Yang, W.; Liu, X.; Yue, X.; Jia, J.; Guo, S. Bamboo-like carbon nanotube/Fe3C nanoparticle hybrids and their highly efficient catalysis for oxygen reduction. *J. Am. Chem. Soc.* **2015,** *137*, 1436-1439.

(51) Liu, X.; Antonietti, M. Moderating black powder chemistry for the synthesis of doped and highly porous graphene nanoplatelets and their use in electrocatalysis. *Adv. mater.* **2013,** *25*, 6284-90.

(52) Liu, D.; Lei, W.; Portehault, D.; Qin, S.; Chen, Y. High N-content holey few-layered graphene electrocatalysts: scalable solvent-less production. *J. Mater. Chem. A* **2015,** *3*, 1682-1687.

(53) Liu, X.; Wang, Y.; Dong, L.; Chen, X.; Xin, G.; Zhang, Y.; Zang, J. One-step synthesis of shell/core structural boron and nitrogen co-doped graphitic carbon/nanodiamond as efficient electrocatalyst for the oxygen reduction reaction in alkaline media. *Electrochim. Acta* **2016,** *194,* 161-167.

(54) Dou, S.; Huang, X.; Ma, Z.; Wu, J.; Wang, S. A simple approach to the synthesis of BCN graphene with high capacitance. *Nanotechnology* **2015,** *26,* 045402.

(55) Lai, L.; Potts, J. R.; Zhan, D.; Wang, L.; Poh, C. K.; Tang, C.; Gong, H.; Shen, Z.; Lin, J.; Ruoff, R. S. Exploration of the active center structure of nitrogen-doped graphene-based catalysts for oxygen reduction reaction. *Energy Environ. Sci.* **2012,** *5,* 7936-7942.

(56) Guo, D.; Shibuya, R.; Akiba,C.; Saji, S.;Kondo, T.; Nakamura, J. ORR Active sites of nitrogen-doped carbon materials for oxygen reduction reaction clarified using model catalysts. *Science* **2016,** *351,* 6271-6275.

(57) Wan, K.; Long, G.; Liu, M.; Du, L.; Liang, Z.; Tsiakaras, P. Nitrogen-doped ordered mesoporous carbon: synthesis and active sites for electrocatalysis of oxygen reduction reaction. *Appl. Catal., B.* **2015,** *165,* 566-571.

(58) Long, G.; Wan, K.; Liu, M.; Li, X.; Liang, Z.; Piao, J. Effect of pyrolysis conditions on nitrogen-doped ordered mesoporous carbon electrocatalysts. *Chin. J. Catal.* 2015, 36, 1197-1204.

(59) Wan, K.; Yu, Z.; Li, X.; Liu, M.; Yang, G.; Piao, J.; Liang, Z. pH effect on electrochemistry of nitrogen-doped carbon catalyst for oxygen reduction reaction. *ACS Catal.* **2015,** *5,* 4325-4332.

1
2
3
4
5
6
7
8
9
10
11
12
13
14
15
16
17
18
19
20
21
22
23
24
25
26
27
28
29
30
31
32
33
34
35
36
37
38
39
40
41
42
43
44
45
46
47
48
49
50
51
52
53
54
55
56
57
58
59
60